The FEBS Journal

FEBS PRESS science publishing by scientists

Single-molecule analysis of dynamics and interactions of the SecYEG translocon

Sabrina Koch[1], Anne-Bart Seinen[1,2], Michael Kamel[3], Daniel Kuckla[4], Cornelia Monzel[4], Alexej Kedrov[3] and Arnold J.M. Driessen[1]

1 Molecular Microbiology, Groningen Biomolecular Sciences and Biotechnology Institute, Zernike Institute for Advanced Materials, University of Groningen, The Netherlands
2 Biophysics, AMOLF, Amsterdam, The Netherlands
3 Synthetic Membrane Systems, Institute of Biochemistry, Heinrich Heine University Düsseldorf, Germany
4 Experimental Medical Physics, Department of Physics, Heinrich Heine University Düsseldorf, Germany

Keywords
fluorescence microscopy; protein folding; protein secretion; protein:lipid interactions; single-molecule analysis

Correspondence
A. Kedrov, Synthetic Membrane Systems, Institute of Biochemistry, Heinrich Heine University Düsseldorf, Universitätsstraße 1, Düsseldorf, Germany
Tel: + 49-211-81-13731
E-mail: kedrov@hhu.de
A. J. M. Driessen, Molecular Microbiology, Groningen Biomolecular Sciences and Biotechnology Institute, Zernike Institute for Advanced Materials, University of Groningen, Nijenborgh 7, Groningen, The Netherlands
Tel: + 31-50-3632164
E-mail: a.j.m.driessen@rug.nl

Sabrina Koch and Anne-Bart Seinen contributed equally

(Received 3 February 2020, revised 11 September 2020, accepted 12 October 2020)

doi:10.1111/febs.15596

Protein translocation and insertion into the bacterial cytoplasmic membrane are the essential processes mediated by the Sec machinery. The core machinery is composed of the membrane-embedded translocon SecYEG that interacts with the secretion-dedicated ATPase SecA and translating ribosomes. Despite the simplicity and the available structural insights on the system, diverse molecular mechanisms and functional dynamics have been proposed. Here, we employ total internal reflection fluorescence microscopy to study the oligomeric state and diffusion of SecYEG translocons in supported lipid bilayers at the single-molecule level. Silane-based coating ensured the mobility of lipids and reconstituted translocons within the bilayer. Brightness analysis suggested that approx. 70% of the translocons were monomeric. The translocons remained in a monomeric form upon ribosome binding, but partial oligomerization occurred in the presence of nucleotide-free SecA. Individual trajectories of SecYEG in the lipid bilayer revealed dynamic heterogeneity of diffusion, as translocons commonly switched between slow and fast mobility modes with corresponding diffusion coefficients of 0.03 and 0.7 $\mu m^2 \cdot s^{-1}$. Interactions with SecA ATPase had a minor effect on the lateral mobility, while bound ribosome:nascent chain complexes substantially hindered the diffusion of single translocons. Notably, the mobility of the translocon:ribosome complexes was not affected by the solvent viscosity or macromolecular crowding modulated by Ficoll PM 70, so it was largely determined by interactions within the lipid bilayer and at the interface. We suggest that the complex mobility of SecYEG arises from the conformational dynamics of the translocon and protein:lipid interactions.

Abbreviations
AFM, atomic force microscopy; CPB, continuous photobleaching; CPD, cumulative probability distribution; CPF, cumulative probability function; DDM, *n*-dodecyl-β-D-maltoside; DOPC, 1,2-dioleoyl-sn-glycero-3-phosphocholine; DOPE, 1,2-dioleoyl-sn-glycero-3-phosphoethanolamine; DOPG, 1,2-dioleoyl-sn-glycero-3-phosphoglycerol; FCS, fluorescence correlation spectroscopy; GUV, giant unilamellar vesicle; IPTG, isopropyl β-D-thiogalactopyranoside; MSD, mean square displacement; PSF, photon spread function; R18, octadecyl rhodamine B chloride; RNC, ribosome: nascent chain complex; RSS, residual sum of squares; SLB, supported lipid bilayer; SRP, signal recognition particle; TIRFm, total internal reflection fluorescence microscopy; TMH, transmembrane helix.

Introduction

About 25–30% of the total bacterial proteins carry out their metabolic and structural function in compartments outside the cytoplasm. The major route for exporting these proteins beyond the cytoplasmic membrane is provided by the essential and universally conserved secretory (Sec) pathway (Fig. 1) [1,2]. The bacterial Sec pathway includes two major targeting routes, which merge at the membrane-embedded protein-conducting channel, or translocon, SecYEG (Fig. 1A). Targeting of membrane proteins commonly occurs co-translationally, and their recognition is based on the presence of a highly hydrophobic N-terminal domain, either a signal sequence or the first transmembrane α-helix (TMH) [3]. Once this signal emerges from the ribosomal exit tunnel, it is recognized and bound by the signal recognition particle (SRP) that facilitates targeting of the ribosome:nascent chain complex (RNC) to the membrane-localized SRP receptor FtsY and then SecYEG translocon [4]. After SRP:FtsY dissociation, the nascent chain is inserted into the SecYEG translocon, and membrane partitioning is facilitated by translation forces of the ribosomes, as well as pulling forces originating from interactions of the nascent chain with the translocon and lipids [5]. Another route is followed by moderately hydrophobic secretory and outer membrane protein precursors (preproteins), which are targeted and translocated post-translationally (Fig. 1B). During preprotein synthesis, the polypeptide emerging from a ribosome is recognized and bound by the ribosome-associated chaperone trigger factor and, possibly, the motor protein SecA [6,7]. Once the synthesis is completed, the preprotein is carried over to the secretion-dedicated chaperone SecB that keeps it in an unfolded, secretion-competent state [8]. In the next step, the preprotein is targeted and transferred to SecA, which is bound to the translocon SecYEG via the cytoplasm-exposed loops 6/7 and 8/9 of the subunit SecY (Fig. 1A), and translocation is initiated [9]. SecA and/or proton motive force may also be required for the translocation of large and polar periplasmic loops within membrane proteins, thus suggesting a dynamic interaction between the translocon and cytosolic components of the targeting pathways [7,10,11].

The majority of translocon structures, as well as many functional studies, have been based on detergent-solubilized proteins, although detergents are known to alter structural and functional properties of proteins [12,13]. Therefore, there is a great demand to perform structural, biochemical and biophysical analysis in physiologically relevant and well-defined systems. Reconstitution of isolated proteins into proteoliposomes remains the most common approach to study membrane proteins, including those of the Sec machinery [14,15], and more recent studies have also used translocons reconstituted in lipid-based nanodiscs [16–20]. Complementary, free-standing and supported lipid bilayers (SLB) offer robust model systems to investigate protein dynamics [21]. SLBs can be formed by fusing lipid vesicles on solid surfaces, such as mica or glass, and can be employed to probe protein:lipid interactions via surface plasmon resonance or quartz crystal microbalance measurements [22], or to carry out surface imaging down to the single-molecule level via atomic force microscopy (AFM) and total internal reflection fluorescence microscopy (TIRFm) [23,24]. Recently, AFM imaging of SecYEG complexes allowed to assign local height increases to the cytoplasm-exposed loops of individual translocons, and to visualize SecYEG:SecA and SecYEG:SecYEG interactions [25]. In an alternative approach, two-dimensional streptavidin crystals were used as a support to form SLBs and to investigate the lateral diffusion of SecYEG using high-speed AFM [26]. This provided insights into conformational changes at the single-molecule level, but the method was not sufficiently fast to analyze the naturally occurring lateral diffusion of proteins, so additional treatment with glutaraldehyde was employed to artificially decrease the diffusion rate of translocons.

Differently to AFM, fluorescence microscopy does not involve mechanical interaction with the examined sample, but also offers single-molecule resolution to monitor the temporal dynamics of membrane proteins [27,28]. Here, we employ TIRFm to study interactions of *Escherichia coli* SecYEG with the cytoplasmic ligands, the ATPase SecA and ribosomes, and to probe their effects on the translocon dynamics and the long-disputed oligomeric state. Single-molecule brightness analysis of SLB-reconstituted translocons suggested that SecYEG complexes remained largely monomeric in their freely diffusing state and when bound to ribosomes, while the assembly of oligomers was stimulated in the presence of SecA. Statistical analysis of single-particle trajectories revealed two distinct diffusion modes of SecYEG within the membrane, and individual translocons could switch between fast and slow diffusion, either in their free state or when bound to ribosomes or SecA, while binding of RNCs drastically suppressed the fast diffusion mode. As the interactions between the SLB and the supporting surface were largely excluded, the nonuniform diffusion pattern in SLBs has been

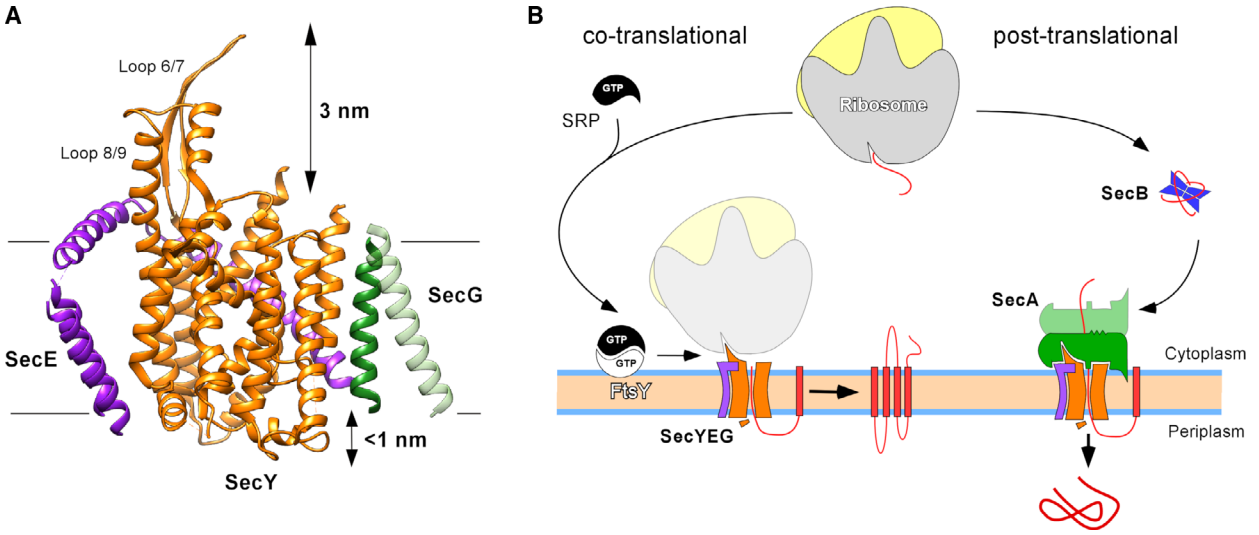

Fig. 1. SecYEG as a hub for protein translocation. (A) Structure of the *Escherichia coli* SecYEG in the lipid bilayer (PDB ID: 6R7L, Ref. [18]). The translocon subunits as well as the approximate heights of the cytoplasmic and periplasmic loops are indicated. The putative position of SecG TMH 1 is shown in light green (PDB ID: 5AWW, Ref. [9]). SecYEG structure is rendered with UCSF Chimera v. 1.13 [72]. (B) Scheme of the co- and post-translational protein targeting to the inner membrane of *E. coli*. The membrane-embedded SecYEG translocon conducts insertion of the nascent membrane proteins delivered in a tertiary complex of the ribosome, SRP, and the membrane-associated receptor FtsY. Secretory and cell wall proteins are delivered to the SecYEG as nonfolded precursors with the help of the dedicated chaperone SecB. The translocation is mediated by the translocon-associated ATPase SecA.

attributed to the conformational dynamics of SecYEG and associated protein:lipid interactions.

Results

Supported lipid bilayers provide the physiologically relevant membrane environment, where dynamics of individual reconstituted translocons, such as association and mobility, can be monitored. However, the setup-specific interactions of proteins and lipids with the supporting surface may hinder their lateral diffusion and so influence the experimental outcome. Direct deposition of SLBs on the solid support would likely result in an intermediate aqueous layer, which may be as thin as 5 Å [29,30]. Indeed, when the SLBs were formed on the bare glass surface, the mobility of lipids was severely suppressed. This was shown by continuous photobleaching (CPB) experiments using dye-conjugated lipids 1,2-dioleoyl-sn-glycero-3-phosphoethanolamine (DOPE)-NBD and recording of diffusion-based signal recovery. On glass surfaces, no signal recovery was recorded even after 20 min (Fig. 2). In contrast, when the glass surface was precoated with a short aminosilane (3-aminopropyl)triethoxysilane (APTES, length below 1 nm) [31], the fluorescence within the bleached areas rapidly recovered due to lipid diffusion. Based on the CPB experiments, a lipid diffusion coefficient of $3.2 \pm 0.4\ \mu m^2 \cdot s^{-1}$ was determined (Fig. 3). This is in a good agreement with previous studies on membrane fluidity [32]. Thus, the short silane spacer reduced the interaction with the solid surface and served to recover the dynamics of the lipids within the bilayer. Importantly, a large mobile fraction of reconstituted translocons was observed within the APTES-supported bilayer (see below), so a relatively small spacing was sufficient to prevent the protein:surface interaction.

To investigate SecYEG dynamics within SLBs and its interactions with SecA ATPase and ribosomes, a TIRFm setup with a mounted flow cell was employed. The flow cell was built from a silane-coated coverslip and an object slide connected via a spacer containing the flow channel. The continuous system allowed the addition of buffer and binding partners to the preformed SLBs, as well as washing off unbound material. To reduce interactions of the periplasmic interface of SecYEG with the glass surface, the glass surface was coated with an elongated aminosilane, *N*-(2-aminoethyl)-3-aminoisobutyldimethylmethoxysilane, of approx. 1.5 nm in length (Fig. 4A). Proteoliposomes bearing SecYEG-Atto 647N translocons were mixed 1 : 250 with protein-free liposomes [14,33], and the mixture was loaded into the flow cell. In presence of 150 mM KCl the liposomes could bind to and spread

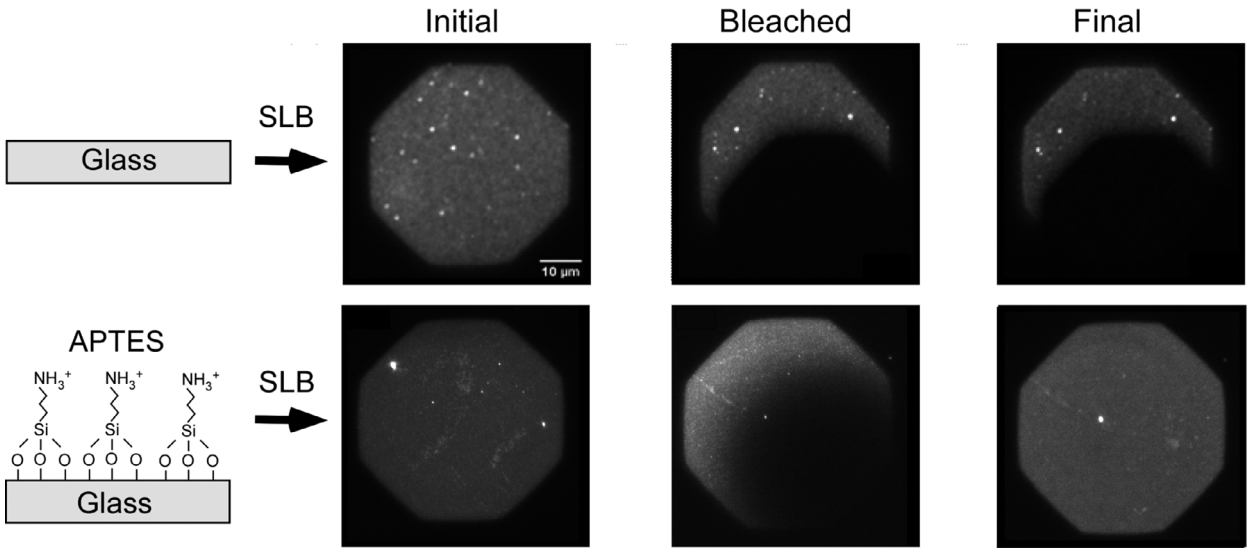

Fig. 2. Silane cushion ensures lipid mobility within the deposited SLB. DOPE-NBD fluorescence recovery after photobleaching was recorded in SLBs deposited on unfunctionalized cleaned glass (top row) and APTES-coated glass surface (bottom row). The 'Initial' image of the formed SLB was recorded before photobleaching and another image was recorded with a lateral shift to differentiate between photobleached and nonphotobleached area ('Bleached'). The fluorescence was allowed to recover over 15–20 min by switching off the lamp, and then, another image was recorded ('Final'). No recovery was detected for SLBs on the bare glass surface indicating an immobile lipid bilayer. Complete recovery of the fluorescence after 20 min was observed for APTES-supported SLBs indicating the mobile bilayer.

over the coverslip due to electrostatic interactions of anionic lipids with positively charged amine group of the silane coat. To verify the proper formation of a lipid bilayer, simultaneous dual-color TIRFm of octadecyl rhodamine B chloride (R18) and SecYEG-Atto 647N was performed (Fig. 4B). R18 is a fluorescent probe, which spontaneously immerses with its alkyl tail into a lipid bilayer, while its polar fluorophore moiety faces the hydrophilic exterior. After the liposomes containing R18 were added to the flow cell, they fused with the deposited SLB, whereupon R18 molecules diffused freely throughout the field of view (Fig. 4C), indicating proper bilayer formation without exclusion zones as a prerequisite for the diffusion analysis.

Site-specific labeling of SecYEG with a small fluorescence dye, such as Atto 647N-maleimide, at the periplasmic interface did not affect the protein activity (Fig. 5A), as the dye did not interfere with SecA and ribosome binding at the cytoplasmic side [33]. The dual topology of reconstituted translocons within the proteoliposomes was confirmed via probing the translocon accessibility for the limited specific proteolysis (Fig. 5B), so two distinct SecYEG populations were expected to be present within SLBs. The brightness distribution of individual particles detected within the SLB was employed to analyze the translocon oligomeric state. Previous biochemical and structural studies have shown that SecYEG complexes may assemble into oligomers in detergent micelles and lipid bilayers [34,35], but a single copy of SecYEG is sufficient to form a functional translocon [16,33,36,37]. To probe the oligomeric state of SecYEG in our experimental setup, the fluorescence intensity of individual foci was analyzed over time to determine the number of translocons per foci (Fig. 5C). SecYEG was predominantly present as a monomer, which built a fraction of approx. 70% of analyzed translocons. Dimers and occasional monomers bearing two fluorophores constituted about 20%, and higher oligomers constituted below 10% of molecules, and the distribution remained stable over the measurement time.

Individual translocons could be detected in consecutively recorded frames, and their trajectories within the SLB were reconstructed (Fig. 6A). About 25% of proteins were mobile, which constituted around 100 proteins per movie, while the rest remained motionless (Fig. 6B). The population of the immobile particles was primarily attributed to the inversely oriented SecYEG, which statistically represented 40–60% of reconstituted translocons within the SLB (Fig. 5B) [14,33]. The inversely oriented translocons exposed their long cytoplasmic loops toward the solid support, so their diffusion could be hindered despite the silane coating (Fig. 1A). Furthermore, occasional protein aggregates and the fluorophore contaminations could

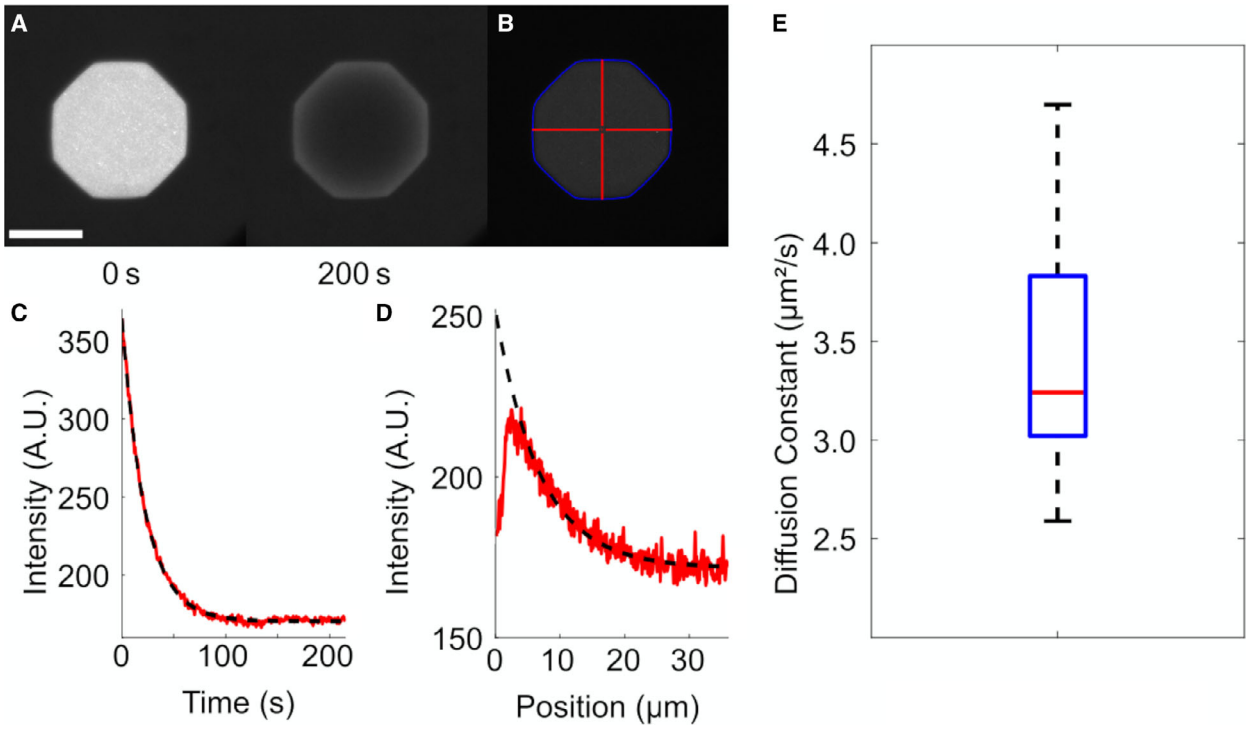

Fig. 3. Verification of SLB mobility utilizing CPB. (A) Fluorescence of DOPE-NBD within SLB deposited on the APTES-coated glass before and after 200 s of bleaching. Scale bar 40 μm. (B) SLB before bleaching with lines indicating the analyzed intensities. From the central point where the lines would intersect, the bleaching constant is determined. Scale as in (A). (C) Mean fluorescence intensity measured at the center spot shown in (B) during the bleaching process. Dashed line: Fit according to Eqn (1), as described in Methods. (D) Mean fluorescence intensity averaged over 5 neighboring pixels along one of the radial lines. Dashed line: Fit according to Eqn (2), as described in Methods. (E) The overall diffusion constant determined for DOPE-DBD lipid amounted to (3.2 ± 0.4) $\mu m^2 \cdot s^{-1}$. Two different samples with a total of $N = 14$ measurements were evaluated. Values represent the median and median absolute deviation ΔD = median($D(i)$ − median(D)).

contribute to the immobile fraction that was excluded from further analysis. The trajectories of the mobile translocons, which contained 5000–10 000 steps per movie, were used to estimate the diffusion coefficients using the cumulative probability distribution (CPD) of step sizes. CPD refers to the probability that a particle stays within a given area around it, thus decreasing the radius r around a moving particle increases the probability that the particle will leave the area determined by r^2. Fitting of the experimentally derived CPD with the cumulative probability function (CPF) provides the number of diffusive species, their fractions and the corresponding diffusion coefficients. Interestingly, the SLB-reconstituted translocons did not diffuse uniformly, but demonstrated clear dynamic heterogeneity (Fig. 6A). SecYEG diffusion could occur in equally distributed short and long step sizes (slow and fast diffusion modes), and individual translocons could switch between these modes. Accordingly, no adequate fitting of the experimental CPD data to a single-component CPF could be achieved, as the goodness of fit indicated by the residual sum of squares (RSS) was larger compared to the two-component CPF fit (Fig. 6C). CPD was best described by the two-component model, and increasing the terms led to overfitting, yielding erroneous fitting parameters, such as equal diffusion coefficients for different components. The median diffusion coefficient of the slow mode was found at 0.029 $\mu m^2\ s^{-1}$, while the fast mode had a median diffusion coefficient of 0.7 $\mu m^2 \cdot s^{-1}$ (Fig. 6D). Notably, two modes with diffusion coefficients of 0.08 and 0.77 $\mu m^2 \cdot s^{-1}$ were also observed for SLB-reconstituted translocons when the short silane APTES was used for coating the glass surface (Fig. 7). Thus, the variations in distance between the SLB and the supporting surface had little effect on the mobility of the translocons, suggesting that the dynamic heterogeneity in SecYEG diffusion was largely determined by the intrinsic interactions within the lipid bilayer.

During translocation of polar polypeptide chains, such as preproteins or periplasmic domains of membrane proteins, SecYEG binds the cytosolic motor

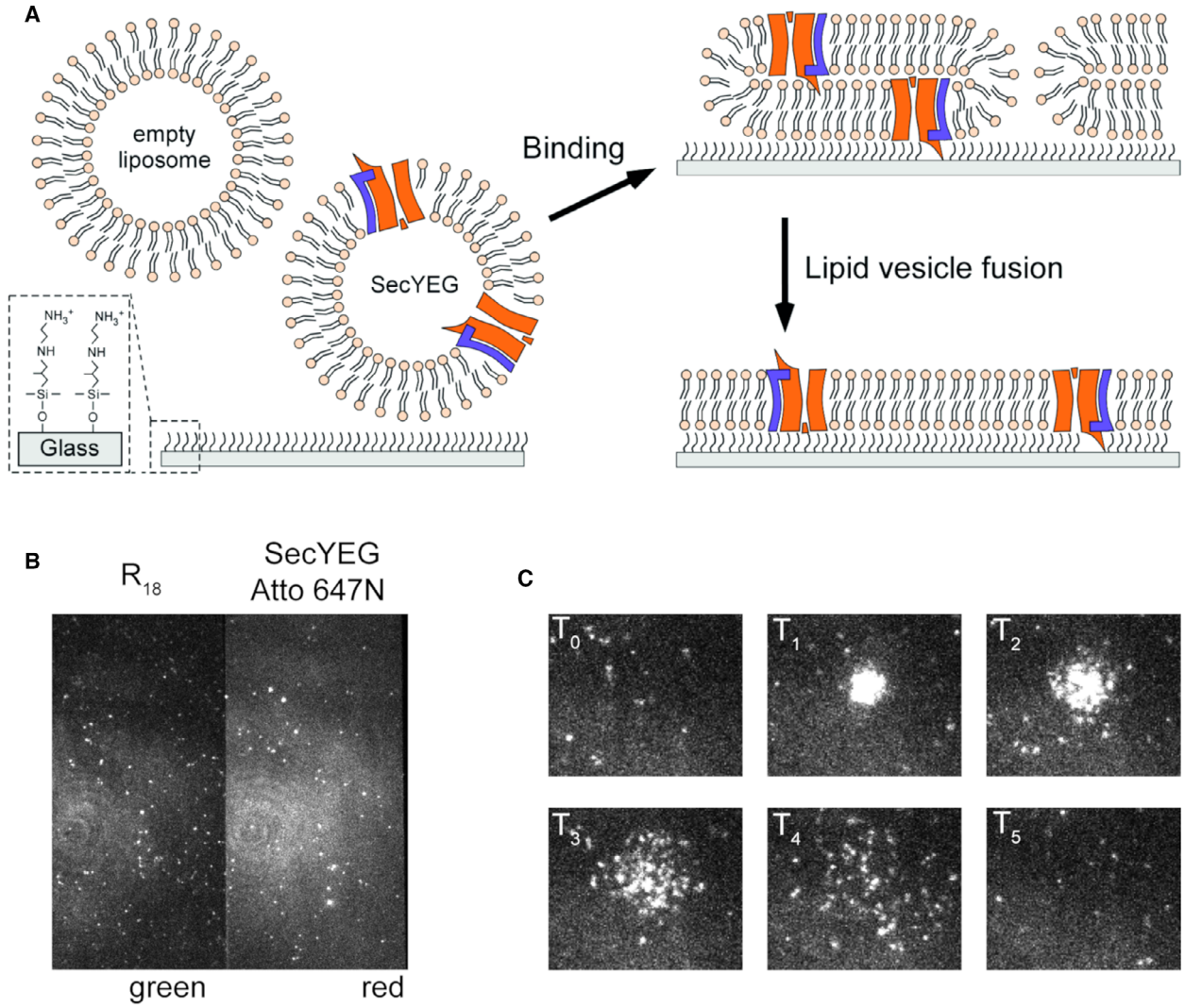

Fig. 4. Preparation of SecYEG-containing SLBs. (A) Scheme of the SLB formation via fusion of SecYEG proteoliposomes and liposomes on the silane-functionalized glass surface. The vesicles bound to the glass-silane surface undergo flattening and fusion to form a continuous lipid bilayer with incorporated translocons. (B) Example frame of the dual-view data acquisition with a beam splitter for green and red channel, detecting R18 and SecYEG-Atto 647N molecules, respectively. (C) Fusion of R18 molecules with the SLB validates the formation of the bilayer. T_0, prior to R18 vesicle fusion. T_1, first contact, R18 vesicle enters the focal plane. T_2, R18 vesicle fusion with the SLB, releasing the R18 molecules into the SLB showing a radial Brownian diffusion pattern. T_3, 66 ms after initial vesicle fusion with the SLB still showing a radial diffusion pattern without exclusion zones. T_4, 99 ms after initial vesicle fusion, R18 molecules start to diffuse out of the imaging boundaries, still in a radial diffusion pattern and without indications of an improper SLB. T_5, diffusion out of the imaging boundaries and bleaching of the R18 molecules resulted in a state similar to T_0, where no local accumulation or exclusion of the dye was observed.

protein SecA. To investigate the effect of SecA binding on the oligomeric state and the diffusion dynamics of SecYEG, the ATPase was introduced to the translocon-containing SLBs. SecA binds SecYEG with high affinity even in the absence of a preprotein [11,17]. The effect of SecA binding could be recognized in raw individual trajectories of SecYEG (Fig. 8A), and CPD analysis revealed a significant change for both slow and fast diffusion modes. The fast diffusion mode revealed a decrease in the diffusion coefficient, from 0.78 to 0.68 $\mu m^2 \cdot s^{-1}$, while the slow-diffusion coefficient increased to 0.033 $\mu m^2 \cdot s^{-1}$ upon SecA addition (Fig. 8B). The brightness analysis suggested that a fraction of the SecYEG underwent dimerization in presence of SecA, as the monomer population reduced to 61% (Fig. 8C).

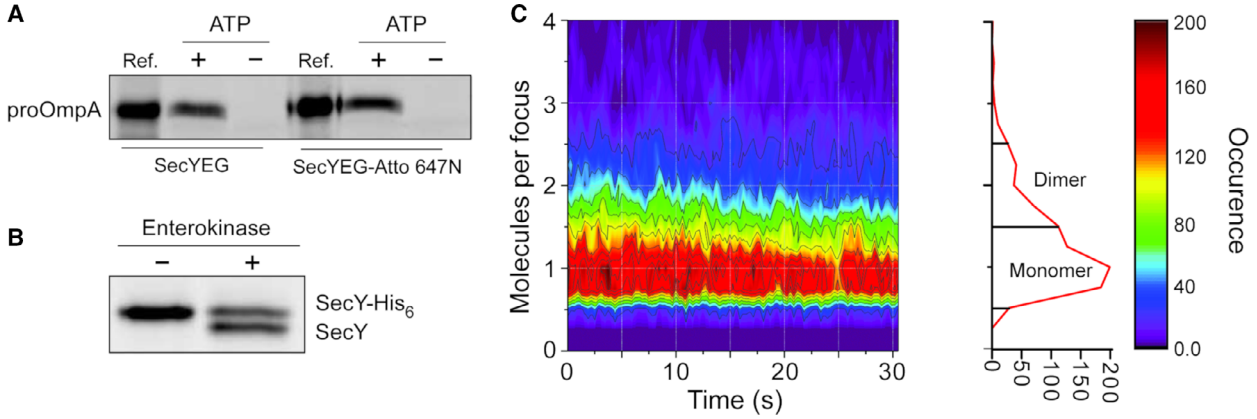

Fig. 5. Characterization of the reconstituted SecYEG translocon. (A) Fluorescent labeling does not affect SecYEG activity. Translocation activities of unlabeled cysteine-free SecYEG translocon and the fluorescently labeled single-cysteine variant $SecY^{C148}EG$-Atto 647N were nearly identical, as comparable amounts of the fluorescently labeled preprotein proOmpA were translocated into proteoliposomes in presence of ATP. 'Ref.' indicates the reference (10% of proOmpA input). (B) Reconstituted translocons acquire alternating orientations in lipid bilayers. Accessibility of SecY N-terminal end for enterokinase cleavage revealed the dual topology of the reconstituted SecYEG. In-gel fluorescence imaging shows a shift of SecY-Atto 647N band upon incubation with the protease. 65% ± 9% of the reconstituted SecYEG exposed the cytoplasmic side the outside of the liposomes ($N = 3$). (C) SecYEG oligomeric state within SLB examined via single-particle brightness analysis. The distribution shows the calculated number of molecules per focus over time. The distribution is largely spread around a single molecule per focus, indicating that the SecYEG translocon in a native-like environment is predominantly monomeric. The ratio of monomers vs dimers was approx. 3 : 1 (15 792 monomeric vs 5663 dimers, based on the full movie). The distribution remained stable over the experimental time span (30 s).

To study the translocon dynamics upon interactions with translating ribosomes and co-translational insertion of a membrane protein, trajectories of SecYEG-Atto 647N were further recorded in the absence and presence of ribosomes. Empty 70S ribosomes did not cause substantial changes in SecYEG diffusion: The individual trajectories showed an unaltered even distribution of short and long step sizes and the diffusion coefficients for two observed modes were weakly affected by ribosomes (Fig. 9A,B), indicating low-affinity transient binding events to SecYEG. Similarly, minor changes in SecYEG diffusion were observed in the presence of RNCs bearing a highly polar nascent chain of the cytoplasmic protein GatD (Fig. 9C). The low affinity of the translocon to GatD-RNC was validated in an independent assay using nanodisc-reconstituted SecYEG. SecYEG was incubated with RNCs containing GatD nascent chain and then centrifuged in continuous density gradient of sucrose (Fig. 9D). While RNCs were found in the center of the gradient (~ 25% sucrose), SecYEG remained in the upper fraction, suggesting that no stable complexes were assembled.

A very different behavior was observed for SecYEG in the presence of FtsQ-RNCs. In this construct, a single TMH of FtsQ was fused at its C-terminal end to the regulatory TnaC sequence, which allowed the stalling of ribosomal translation [38]. The complete FtsQ TMH exposed from the ribosomal exit tunnel allowed for an interaction with the Sec translocon even in the absence of cellular targeting factors, as validated by the centrifugation in the sucrose density gradient (Fig. 9D) [11,18]. The complex assembly was then probed via single particle tracking in SLBs. While the ribosome-free SecYEG manifested the switch between diffusion modes (diffusion coefficients 0.025 and 0.70 $\mu m^2 \cdot s^{-1}$), in the presence of 50 nM FtsQ-RNCs, the coefficient of the fast diffusion decreased by ~ 30% to 0.48 $\mu m^2 \cdot s^{-1}$, while the slow-diffusion coefficient rose to 0.034 $\mu m^2 \cdot s^{-1}$ (Fig. 10A). Importantly, upon adding FtsQ-RNCs, the long step sizes, which largely contributed to the fast diffusion mode, also became less abundant and the decrease of the diffusional mobility of SecYEG upon RNC binding could be directly seen in individual trajectories (Fig. 10B). Thus, we concluded that stable nascent chain-specific assembly of SecYEG : RNC led to pronounced differences in the translocon mobility. As no changes in the brightness of the observed foci were detected (Fig. 10C), the translocons remained monomeric also in complex with RNCs, in agreement with the available structural data [18].

The prominent effect of FtsQ-RNC on SecYEG diffusion could potentially originate from the increased

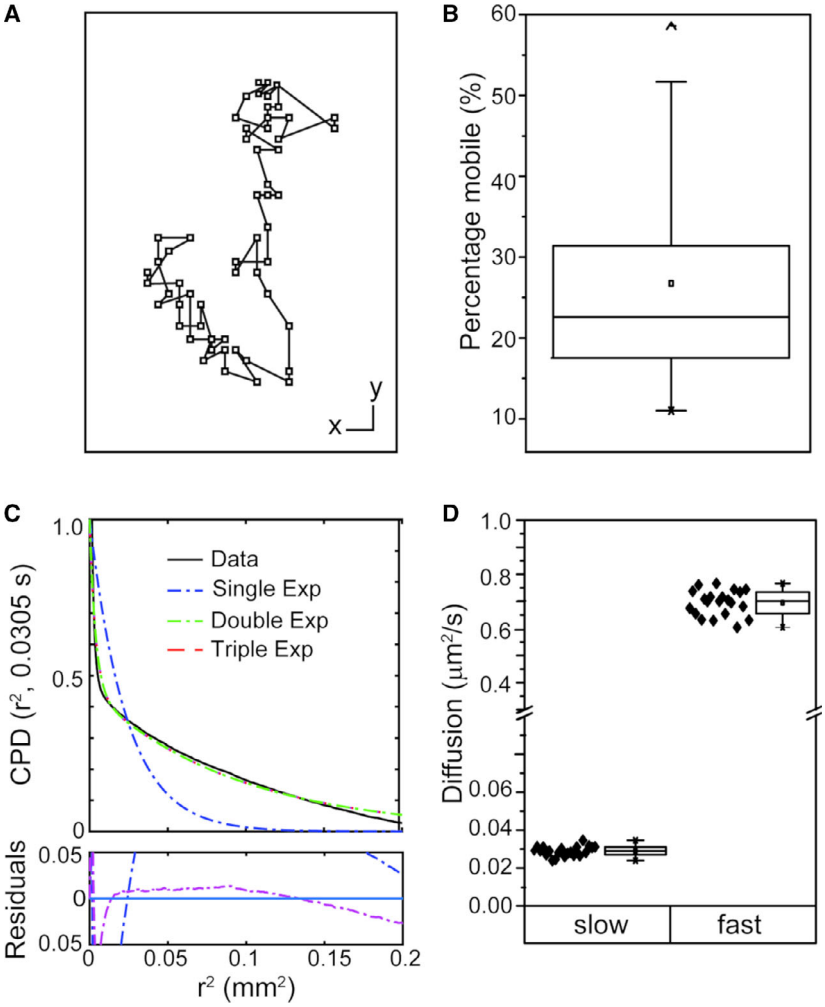

Fig. 6. Tracking of single SecYEG translocons in SLBs. (A) A representative diffusion trajectory of a single SecYEG-Atto 647N molecule. Heterogeneous step sizes are observed. Scale bars for the lateral displacements (*x*, *y*) correspond to 0.5 μm. (B) Percentage of mobile SecYEG particles within the silane-supported SLB. Box plot was created from 40 independent movies, the median was found at 22.6%. The immobile fraction was assigned to the inverted translocons, but also occasional aggregates and fluorescent contaminations. (C) CPD analysis of SecYEG diffusion included fitting of the data to different CPFs containing either one, two, or three components. The corresponding residuals (panel below) indicate that the single-component CPF cannot be applied to analyze SecYEG diffusion. (D) Two diffusion modes of translocons with median diffusion coefficients of 0.03 and 0.7 $\mu m \cdot s^{-2}$ were revealed. Each dot corresponds to a value acquired from an individual movie.

mass and the large solvent-exposed volume of the assembled complex, or from interactions within the SLB, such as distortion of the lipid bilayer or the translocon conformation. According to Saffman-Delbrück model, diffusion of the membrane-embedded translocon is determined by the viscosity of the lipid bilayer and, to a less extent, the viscosity of the aqueous phase [39]. Thus, changing the viscosity of the aqueous phase would reveal the contribution of the peripherally bound ribosome. The buffer viscosity may be tuned by Ficoll, a chemically inert hydrophilic polysaccharide commonly employed to mimic the intracellular crowding [40]. Ficoll PM 70 did not hinder SecYEG:RNC interactions, as it was validated using nanodisc-reconstituted translocons (Fig. 11A). To probe the effect of the buffer viscosity on SecYEG diffusion in SLBs, tracking experiments were repeated in the presence of 40 % (w/v) Ficoll PM 70. The high concentration of Ficoll PM 70 in solution did not affect the diffusion of free SecYEG in SLBs, so the solvent-exposed loops did not influence the mobility of the integral membrane protein (Fig. 11B). Importantly, the elevated viscosity in solution did not affect the lateral diffusion of SecYEG:RNC complexes assembled at the SLB interface. Thus, the solvent:ribosome interactions had a weak effect on the lateral mobility of the SecYEG:ribosome complex within the SLB, and the hindered diffusion was likely determined by protein: lipid interactions and the conformation of the membrane-embedded translocon.

Discussion

Despite the extensive biochemical, biophysical and structural analysis, functional dynamics of the universally conserved Sec translocon in the lipid membrane environment remain challenging to understand. Aiming for physiologically relevant insights on the

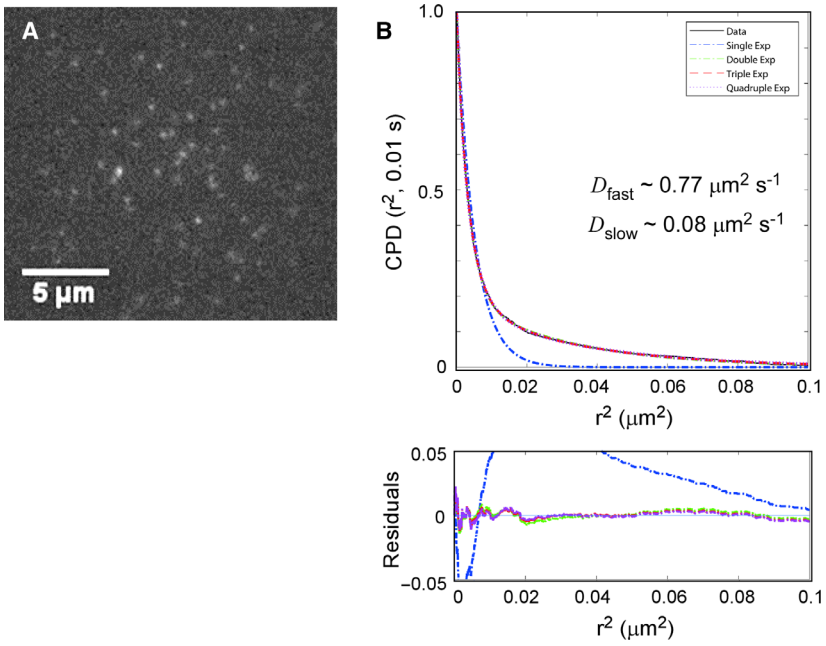

Fig. 7. Mobility of SecYEG in APTES-SLBs. (A) Observation of individual SecYEG-Atto 647N translocons in wide-field microscopy experiments. (B) CPD analysis of SecYEG diffusion suggests two distinct modes (slow and fast) with approx. 10-fold different diffusion coefficients, which match closely those observed for SLBs formed on longer silane variant *N*-(2-aminoethyl)-3-aminoisobutyldimethylmethoxysilane.

translocon dynamics, fluorescence correlation spectroscopy (FCS) and cryo-electron microscopy have been previously employed to probe SecYEG:ribosome and SecYEG:SecA interactions in lipid-based nanodiscs and giant unilamellar vesicles (GUVs) [11,16,18,33,41]. Complementary to those highly sensitive methods, single-molecule detection of translocons should allow probing the properties of individual molecules within the ensemble and potentially revealing the heterogeneity in molecular dynamics [25,26]. With this goal, we have established the fluorescence-based tracking approach to investigate SecYEG diffusion and the oligomeric state at the single-molecule level and to investigate how interactions with SecA and ribosomes modulate the translocon.

In contrast to GUVs, SLBs are easier to prepare and they are not sensitive to axial movement of the membrane caused by membrane undulations [42] and translocation activity of SecYEG within mica-deposited SLBs has been recently reported [25]. To reproduce the native fluidity of both leaflets of the bilayer, SLBs should allow lateral mobility of lipids and embedded translocons [43]. Interactions of SLBs with the solid support cannot be excluded once the lipid membrane is deposited directly on glass. Our data show that the thin aqueous layer of ~ 5 Å formed between the lipid bilayer and the supporting surface [29,30,44,45] was not sufficient to ensure lateral diffusion within the SLB, in agreement with previous reports for DOPE-containing SLBs [46]. Introducing a short silane coating APTES recovered the lateral mobility of lipids and reconstituted translocons, wherefore sufficient spacing was provided to avoid the interaction of SLBs with the surface underneath. The elongated silane-derivate coating was then implemented to prevent contacts between the surface and the short periplasmic loops of SecYEG [9,26], while the cytoplasmic interface of the translocon was exposed to the aqueous solvent, being accessible for interactions with ribosomes and SecA. Inversely oriented and so inactive translocons may contact the surface with the long structured cytoplasmic loops 6/7 and 8/9 of SecY. These loops extend up to 3 nm beyond the membrane interface, so their lateral diffusion may be hindered even in presence of the silane spacer. We believe that these inversely oriented SecYEG largely determined the fraction of the immobile particles observed within SLBs, as they constitute approx. 50% of translocons within the bilayer due to the stochastic orientation of the reconstituted proteins [14,33]. Under this feasible assumption, the performed SLB-based mobility analysis allowed segregating translocons in the nonrelevant membrane topology, as well as occasional aggregates, at the single-molecule level and focusing on the properties of the functionally oriented proteins.

Tracking individual translocons within the SLB revealed the dynamic heterogeneity in their diffusion, as the protein displacement could occur either in short (~ 50 nm) or long (200–300 nm) steps, making the conventional mean square displacement analysis (MSD) challenging [47]. Instead, a multicomponent

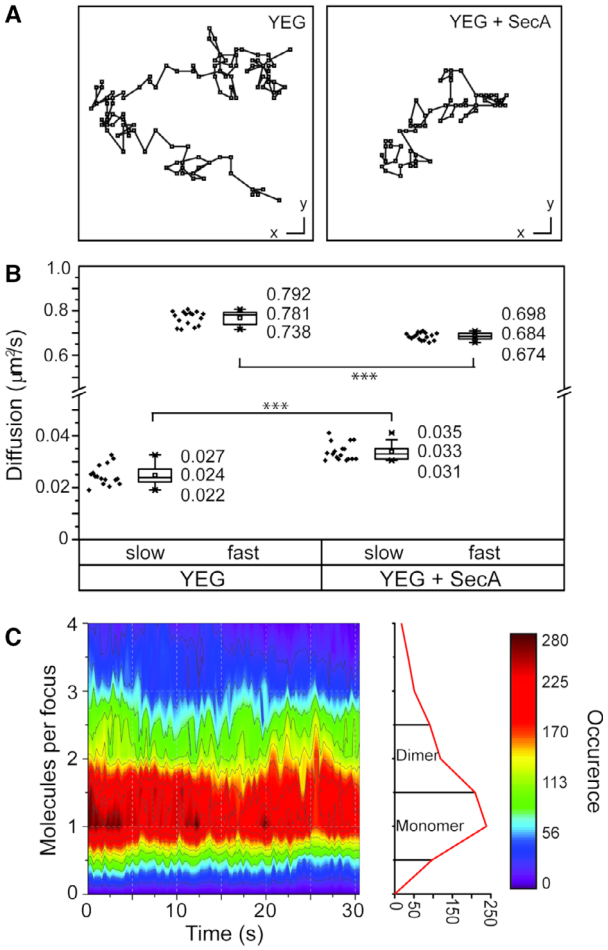

Fig. 8. SecYEG diffusion in the presence of SecA. (A) Representative trajectories of a single SecYEG-Atto 647N molecule alone and in the presence of SecA. Scale bars correspond to 0.5 μm. (B) In the presence of SecA SecYEG the slow-diffusion coefficient increased from 0.024 to 0.033 $\mu m \cdot s^{-2}$, while the fast diffusion coefficient decreased from 0.78 to 0.68 $\mu m \cdot s^{-2}$. ***indicates $P < 0.0005$ in a *t*-test. (C) Single-molecule analysis reveals higher heterogeneity in SecYEG brightness, which may indicate partial dimerization of translocons. The ratio of monomers vs dimers was approx. 2.5 : 1 (52 399 monomeric vs 21 545 dimers, based on the full movie).

CPD analysis suggested that two diffusion modes of SecYEG differed by their instant diffusion coefficients approx. 20-fold, 0.03 and 0.7 $\mu m^2 \cdot s^{-1}$. Recently, the AFM-based study demonstrated that the heterogeneity in SecYEG diffusion may occur in the presence of local confinements at the membrane interface, in agreement with the 'picket-fence model' [26,48]. However, the origin of the heterogeneity within the homogeneous SLB is less clear. The experiments performed with the silane coatings of different length suggested that the supporting surface had minor effect on SecYEG mobility. One possible explanation for the nonuniform diffusion behavior might be provided by transient interactions within the SLB. Complex diffusion patterns within model membranes have been described for lipids and lipid analogues [43,49], but also transmembrane peptides [50], and assigned either to subdiffusion within specific lipid clusters or formation of protein : lipid assemblies with altered diffusional properties. Furthermore, the shape of the transmembrane protein and the occasional hydrophobic mismatch between a membrane protein and the lipid bilayer greatly affects the lateral mobility and causes deviations from Saffman-Delbrück model [51,52]. Specific interactions of SecYEG with anionic phospholipids have been recently described [18,53,54], and the designed SLBs contained 30 mol% 1,2-dioleoyl-sn-glycero-3-phosphoglycerol (DOPG) to mimic their naturally abundant content. While it is unlikely that DOPG lipids segregate within the formed SLBs, dynamic association/dissociation of lipids from the translocon interface may cause conformational changes within SecYEG and alter its lateral mobility. Structural rearrangements may involve peripheral and lipid-exposed domains, such as TMHs 1 and 2 of SecE and the complete SecG subunit, which are highly dynamic as judged from biochemical and structural data [9,18,55,56]. When being re-positioned within the translocon, those peripheral domains would cause a substantial change in the shape of the translocon or cause distortions in the lipid packing, which determine the lateral diffusion within the highly viscous lipid membrane [39,51,52].

Empty 70S ribosomes and ribosomes loaded with the highly polar nascent chain of GatD had modest effect on the translocon lateral diffusion, as it is readily explained by low affinity, transient binding events, and lack of ribosome : lipid interactions [11]. Upon addition of FtsQ-RNCs, the diffusion rate of SecYEG decreased by 30%, indicating that binding of FtsQ-RNCs reduces the lateral mobility of translocons. As diffusion of the SecYEG:FtsQ-RNC complex was not sensitive to the viscosity of the aqueous phase, it was rather determined by the interactions at the lipid interface and within the membrane, than by the shear imposed by the bound ribosome. Interestingly, the ribosome does not only bind to loops 6/7 and 8/9 of SecY, but may also interact with surrounding lipids near the translocon lateral gate. The rRNA helix H59 was observed in a direct contact with lipid head groups and was suggested to recruit anionic phospholipids and disorder the lipid bilayer to assist the insertion of nascent membrane proteins [57]. Those

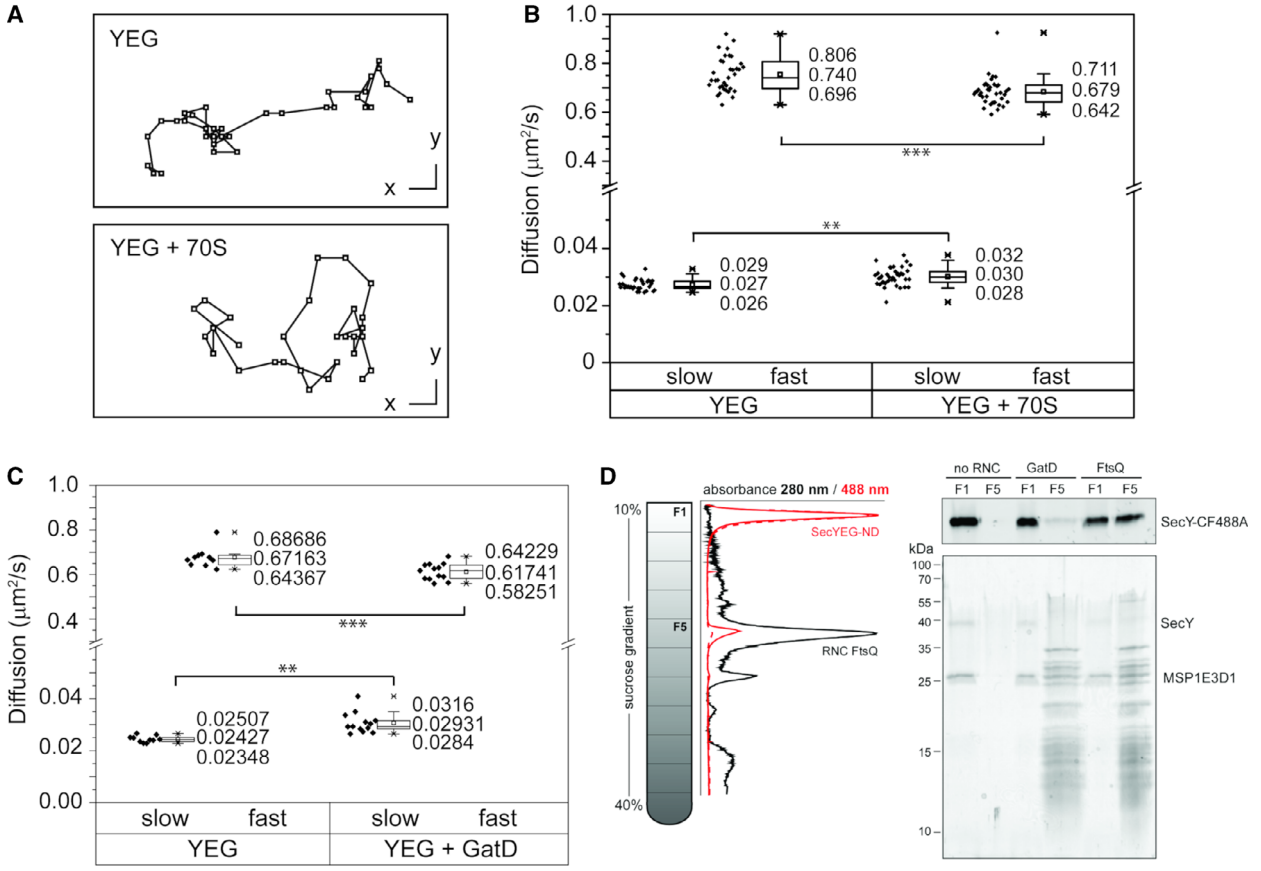

Fig. 9. SecYEG diffusion in the presence of ribosomes. (A) Representative trajectories of single SecYEG-Atto 647N molecules alone and in the presence of 70S ribosomes. Scale bars correspond to 0.5 μm. (B) In the presence of nontranslating 'empty' ribosomes ('70S') the fast diffusion coefficient reduces from 0.74 to 0.68 $\mu m \cdot s^{-2}$. ** indicates $P < 0.005$, and *** indicates $P < 0.0005$ in a *t*-test. (C) In presence of polar GatD-RNCs the fast diffusion coefficient reduces from 0.67 to 0.61 $\mu m \cdot s^{-2}$. Thus, both empty ribosomes and GatD-RNCs have minor effect on the lateral mobility of the translocons. (D) SecYEG : RNC assembly is sensitive to the nascent chain polarity. Nanodisc-reconstituted SecYEG was incubated with RNCs containing GatD (polar) or FtsQ (apolar) nascent chains. The complex assembly was probed via centrifugation in sucrose density gradients. Left: UV-Vis profiles and collected fractions of sucrose density gradients. For FtsQ-RNC sample, the absorbance of SecYEG-conjugated CF488A dye (solid red line) correlated with the strong UV absorbance of RNCs (black line), indicating that a fraction of SecYEG-nanodiscs was bound to these RNCs. No correlation was observed between GatD-RNC and SecYEG-nanodiscs (dashed red line), indicating weak or no binding. Right: SDS/PAGE of selected fractions F1 (no sucrose) and F5 (25% sucrose) collected for free SecYEG-nanodiscs ('no RNC') and SecYEG in presence of GatD and FtsQ-RNCs. In-gel fluorescence visualizes the distribution of SecY-CF488A (top). To avoid the fluorescence signal saturation, fraction F1 load was reduced to 10%. The nanodisc-forming protein MSP1E3D1 is indicated on Coomassie-stained SDS-PAGE (bottom).

ribosome:bilayer interactions, as well as conformational changes involving SecE and SecG subunits, would further affect the diffusion of the translocon.

A moderate decrease in the diffusion coefficient of SecYEG detected upon SecA binding correlates with previous results acquired by means of FCS on free-standing membranes of GUVs [33]. Crystal structures of the SecA:SecYEG complex reveal that SecA interacts with loop 6/7 and loop 8/9 of SecY, which are the same binding sites as for ribosome binding [11,57,58]. Additionally, SecA was shown to interact with lipids, in particular anionic phospholipids: The amphipathic N-terminal helix of SecA anchors at the lipid bilayer interface, which activates SecA for high affinity binding to the translocon [17,59,60]. Despite these SecA:lipid interactions, binding of the motor protein did not affect the translocon diffusion as much as binding of FtsQ-RNC, which can be explained by a smaller surface area involved in SecA:SecYEG:lipid contact and minor structural rearrangements within SecYEG in absence of the substrate preprotein [58]. Also, the less pronounced effect on the translocon diffusion might be due to transient association and dissociation of SecYEG : SecA complex in the absence of nucleotides

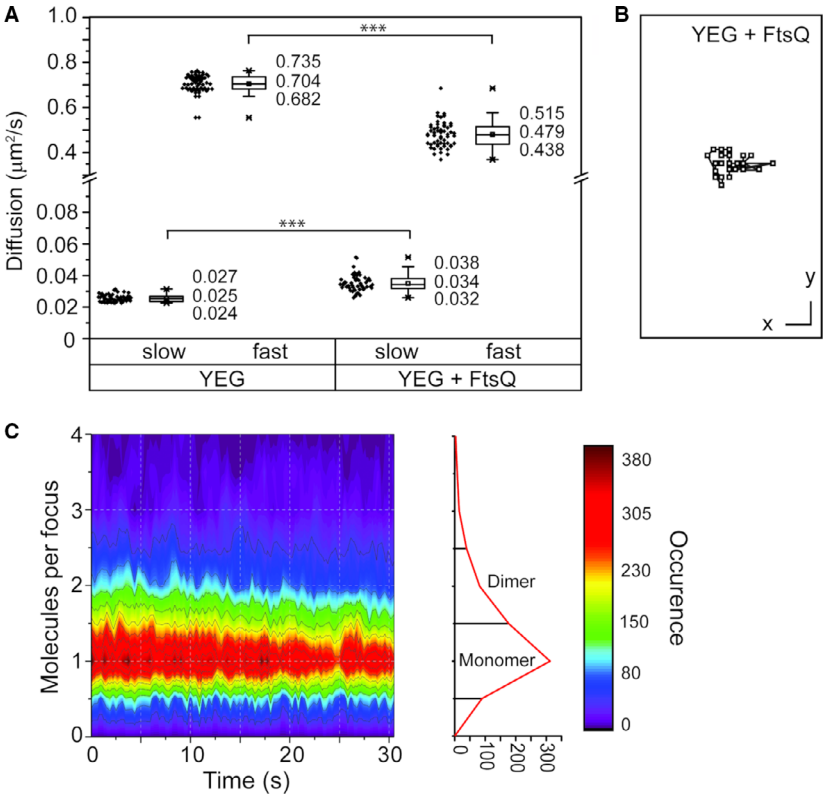

Fig. 10. Tight docking of ribosomes affects the mobility of SecYEG. (A) In the presence of translation-stalled FtsQ-RNCs the fast diffusion coefficient of SecYEG drops from 0.7 to 0.48 μm·s^{-2}. (B) A representative trajectory of single SecYEG in the presence of FtsQ-RNCs reflects the hindered diffusion of the ribosome-bound translocon. (C) Brightness distribution of single translocon foci reveals that SecYEG remains monomeric upon interactions with FtsQ-RNCs. The ratio of monomers vs dimers was approx. 4 : 1 (56 582 monomeric vs 14 290 dimers, based on the full movie).

[33,58]. As single-molecule analysis suggested a broader distribution of translocon brightness in presence of SecA, partial dimerization of SecYEG could occur under these conditions [16,33]. It should be noted, however, that the putative oligomeric assemblies contained multiple translocons and may contain a major fraction of SecYEG. The functional role of the dimerization is not clear, as monomers of SecYEG were shown to form active translocons *in vitro* and *in vivo* [16,33,41,61].

Single-molecule observations of biological processes allow describing complex molecular mechanisms in

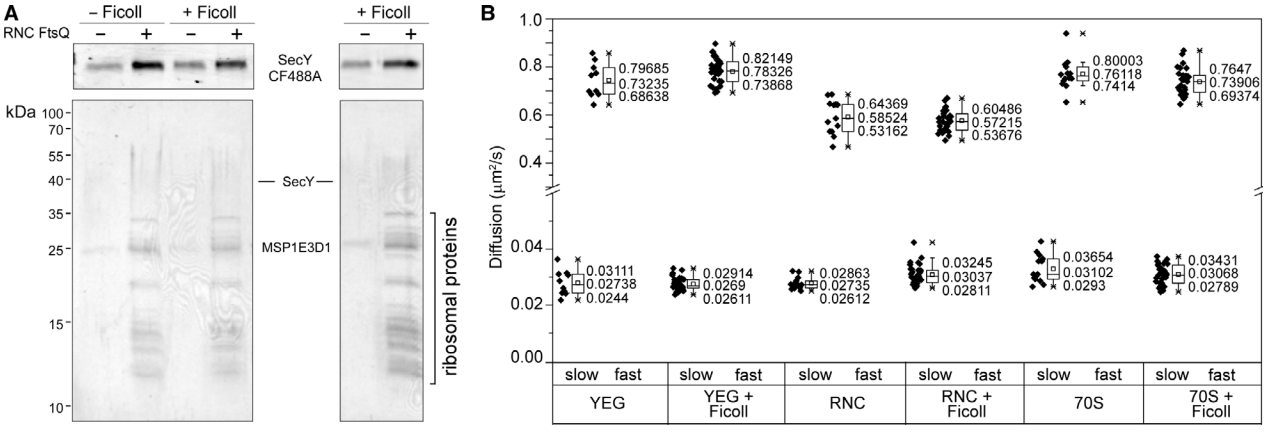

Fig. 11. The buffer viscosity does not affect diffusion of SecYEG and SecYEG : ribosome complexes. (A) The elevated viscosity and macromolecular crowding induced by polysaccharide Ficoll does not prevent SecYEG : ribosome interactions. FtsQ-RNCs bind nanodisc-reconstituted SecYEG in presence of 40% (w/v) Ficoll PM 70 and pellet as a complex through the sucrose cushion. Top: In-gel fluorescence of SecY-CF488A; bottom: Coomassie-stained SDS-PAGE showing SecYEG-ND bands and the pattern of ribosomal proteins. (B) Ficoll PM 70 at concentration 40% (w/v) does not affect the mobility of free or ribosome-bound SecYEG.

unprecedented details, revealing individual pathways and hidden intermediate states. Here, we describe the first fluorescence-based single-molecule analysis of the translocon SecYEG in SLBs and demonstrate its applicability to investigate not only diffusion, but also interactions of individual translocons with ribosomes and SecA in real-time. SLB-reconstituted SecYEG was found predominantly in monomeric form, and could also bind RNCs as a monomer, though a partial dimerization was observed in presence of SecA motor protein. Surprisingly, substantial dynamic heterogeneity was observed in diffusion trajectories of single SecYEG molecules that was attributed to transient translocon:lipid interactions and the conformations dynamics of SecYEG. Our data revealed a strong effect of RNC binding on the diffusional characteristics of the SecYEG complex, which is can be related to SecYEG:lipid and ribosome:lipid interactions, and/or conformational changes within the translocon. Further, the work provides benchmarking values of membrane diffusion rates of various complexes of SecYEG that will facilitate interpretation and analysis of the diffusion of the translocon, also in living cells.

Methods

Protein purification and labeling

SecA was overexpressed in *E. coli* BL21 (DE3) cells carrying the pTrc99A-SecA plasmid and purified as described [17,62]. $SecY_{C148}EG$ was overexpressed in *E. coli* SF100 and C41(DE3) cells carrying the pEK20-C148 plasmid [33] and isolated from crude membranes as described [14]. The translocon was labeled at the unique periplasmic cysteine in position 148 upon incubation with 100 μM Atto 647N-maleimide (Atto-Tec GmbH, Siegen, Germany) or CF488A-maleimide (Biotium Inc., Hayward, CA, USA) as described [17]. Protein concentrations and the labeling efficiency were determined spectrophotometrically using the corresponding extinction coefficients at 280 nm: SecA—75 750 $M^{-1}{\cdot}cm^{-1}$, SecYEG—71 000 $M^{-1}{\cdot}cm^{-1}$ at 280 nm, CF488A—70 000 $M^{-1}{\cdot}cm^{-1}$ at 490 nm, and Atto 647N—150 000 $M^{-1}{\cdot}cm^{-1}$ at 647 nm.

Lipid preparation

A mixture of chloroform-dissolved lipid DOPG:DOPE:1,2-dioleoyl-sn-glycero-3-phosphocholine (DOPC; Avanti Polar Lipids Inc., AL, USA) was prepared at the molar ratio 30:30:40 [33]. DOPG concentration of 30 mol % was used to mimic the anionic lipid content of the cytoplasmic membrane of *E. coli*, while the zwitterionic lipid DOPC facilitated the stability of the planar SLB. The chloroform was evaporated under a nitrogen stream, after which chloroform remnants were extracted overnight under vacuum conditions using a desiccator. The resulting lipid film was resuspended in 20 mM HEPES/KOH pH 7.5, 2 mM DTT to obtain final lipid concentration of 10 $mg{\cdot}mL^{-1}$.

Reconstitution of SecYEG into proteoliposomes

Liposomes were diluted to 4 $mg{\cdot}mL^{-1}$ using a buffer containing 20 mM HEPES/KOH pH 7.5, 50 mM KCl, 0.5% Triton X-100, and 0.05% *n*-dodecyl-β-D-maltoside (DDM). Lipids were incubated for 15 min at 37 °C and subsequently 15 min on ice. SecYEG-Atto 647N (final concentration 200 nM) was added to 1 mL of the lipid : detergent mixture (1 : 30 000 protein-to-lipid ratio) and incubated for 30 min at 4 °C. The detergent was removed in three steps of 1.5 h with 50, 75, and 100 mg Bio-Beads SM2 sorbent (Bio-Rad Laboratories GmbH, Düsseldorf, Germany), whereby the last incubation was performed overnight. Translocon functional activity was validated in translocation assay in proteoliposomes using preprotein proOmpA labeled with BDP-FL-maleimide (Lumiprobe GmbH, Hannover, Germany) as a substrate [63]. Topology of reconstituted SecYEG was probed based on the accessibility of the N-terminal cleavage site within SecY for the enterokinase [14]. Proteoliposomes were incubated with eight units of the enterokinase light chain (New England Biolabs GmbH, Frankfurt/Main, Germany) overnight at 25 °C. The cleavage efficiency was evaluated based on the shift of SecY band in SDS/PAGE.

Reconstitution of SecYEG into nanodiscs

The reconstitution was performed following the previously established protocols [16,18]. Briefly, purified and fluorescently labeled SecYEG translocons in DDM were mixed with MSP1E3D1 major scaffold proteins and detergent-solubilized DOPG:DOPE:DOPC lipids at the molar ratio 1:10:500. Spontaneous nanodisc formation was achieved upon the detergent removal with Bio-Beads SM2 sorbent. SecYEG-loaded nanodiscs were separated from empty nanodiscs via size-exclusion chromatography using Superdex 200 10/300 Increase column and AKTA Pure system (GE Healthcare Life Sciences, MA, USA) in 150 mM KOAc, 5 mM $Mg(OAc)_2$, 25 mM HEPES pH 7.4, and cOmplete protease inhibitor cocktail (Roche, Basel, Switzerland).

RNC isolation

TnaC-stalled RNCs were prepared *in vivo* and isolated as previously described [18,64]. Briefly, KC6Δ*ssrA*Δ*smpB* cells [65] were used to synthesize poly-histidine-tagged fragments of FtsQ and GatD proteins followed by the TnaC sequence that caused stalling of the ribosomal translation at elevated

tryptophan concentrations [38], so stable and well-defined RNCs could be formed. N-terminal poly-histidine tags of the nascent chains were employed for Ni-NTA-based purification of RNCs, and assembled RNCs were further isolated by centrifugation in continuous 10–40% sucrose gradients (Gradient station, Biocomp Instruments, Fredericton, Canada). Presence of the tRNA-linked nascent chains was validated via the tag-specific western blotting. For preparing empty ribosomes, a crude ribosome extract from nontransformed KC6 cells was incubated in presence 1 mM puromycin for 30 min on ice to release nascent chains, and fully assembled 70S ribosomes were isolated via sucrose gradient, as described above.

SecYEG : RNC binding in nanodiscs

Two-hundred nanomolar CF488A-labeled translocons reconstituted into nanodiscs were optionally incubated with 200 mM FtsQ- or GatD-RNC for 30 min at the ambient temperature, loaded on top of continuous 10–40% sucrose gradients in SW40-type tubes and centrifuged 160 000 g for 3 h at 4 °C. The gradients were fractionated from top to the bottom with Gradient station (Biocomp Instruments) in fractions of 1 mL, while continuously recording absorbance at 280 and 488 nm. Contents of individual fractions were precipitated in 15% (w/v) trichloracetic acid and analyzed on SDS-PAGE by recording in-gel fluorescence and Coomassie-stained proteins (AI680 RGB imager; GE Healthcare Life Sciences). To probe the effect of Ficoll PM 70 on SecYEG:RNC interactions, 200 nM nanodisc-reconstituted SecYEG-CF488A was prepared in 40% (w/v) Ficoll 70, and then, 200 nM FtsQ-RNC were added. The reaction was incubated for 30 min at the ambient temperature, then rapidly diluted twofold with the nanodisc buffer, loaded above the sucrose cushion [1 M sucrose, 150 mM KOAc, 5 mM $Mg(OAc)_2$, 25 mM HEPES pH 7.4, and protease inhibitor cocktail (Roche)] and centrifuged in S120-AT3 rotor (Sorvall/Thermo Fisher, Waltham, MA, USA) at 60 000 g for either 20 or 40 min, 4 °C. Pellets were collected and analyzed on SDS-PAGE.

Glass functionalization and flow cell preparation

For SLB formation several requirements are essential: Firstly, the surface has to be cleaned vigorously in order to eliminate organic adsorbents and other contaminants, such as dust [24]. Secondly, a critical concentration of vesicles has to be supplied to the surface to initiate vesicle rupture and subsequent SLB formation. Crowding most likely enhances the interaction between vesicles, which induces stress and rupture [66]. Thirdly, to support SLB formation for vesicles harboring negatively charged lipids, such as DOPG, high ionic strength buffers are necessary [67]. Glass for microscopy was sonicated in acetone at 30 °C for 30 min followed by rinsing the glass six times with deionized water. Next, the coverslip surface was activated by sonicating for 45 min at 30 °C in 5 M KOH. Afterward, traces of KOH were removed by rinsing six times with deionized water, followed by drying the glass for 30 min at 110 °C. Glass surfaces were plasma cleaned for 10 min prior to the surface functionalization with 2% (v/v) *N*-(2-aminoethyl)-3-aminoisobutyldimethylmethoxysilane (abcr GmbH, Karlsruhe, Germany) for 1 hour at room temperature. Afterward, the coverslips were rinsed once with acetone and subsequently dried with pressurized air and stored overnight under vacuum. Prior to each microscopy experiment, a flow cell was constructed by cutting out a channel from a piece of double-sided tape (75 × 25 mm) and fixed to a cleaned object slide containing inlet and outlet holes. The flow cell was formed by placing the object slide on top of a functionalized cover slip. Tubing was inserted into the inlet and outlet openings and fixed with epoxy glue.

The glass functionalization procedure was slightly modified for coating with APTES. Briefly, APTES was dissolved in water to a final concentration of 2%, the pH was then adjusted to three using HCl. The functionalized glass cover slides were then immersed in the silane solution and incubated for 2 h at 75 °C. The glass cover slides were then washed with the deionized water and stored in water until used.

Supported lipid bilayer generation

Liposomes were diluted to 4 $mg{\cdot}mL^{-1}$ using a buffer containing 50 mM HEPES/KOH, pH 7.5, and 50 mM KCl and sonicated in an ultra-sonic bath (Sonorex Super; Bandelin, Berlin, Germany) for 15 cycles alternating between on/off stages, each of 15-s duration, to form small unilamellar liposomes. Protein-free liposomes were mixed with proteoliposomes containing SecYEG (final SecYEG concentration 50 pM, protein-to-lipid ratio below 1 : 5 000 000). The flow cell chamber was washed with 50 mM HEPES/KOH pH 7.5, 50 mM KCl at a flow rate of 10 $\mu L{\cdot}min^{-1}$ prior injecting the SecYEG proteoliposome/liposome mixture. The fusion of the SecYEG proteoliposomes/liposomes on the surface, which thereby form an SLB, was induced by elevated salt concentrations in a washing step using 50 mM HEPES/KOH pH 7.5 and 150 mM KCl. Unbound material was washed out of the flow cell chamber with 50 mM HEPES/KOH pH 7.5, 50 mM KCl. 2D diffusion of R18 was monitored for every experiment to validate reliable SLB formation and diffusion analysis. To investigate SecYEG binding, the concentration of added FtsQ-RNCs, SecA, 70S ribosomes and GatD was 50 nM.

Wide-field microscopy

For single-particle tracking and CPB an epifluorescence microscope (IX73 Olympus, Tokyo, Japan) in combination with an 100× oil-objective (Apochromat & TIRF, NA 1.45;

Olympus) was used. All images were captured with a back-illuminated sCMOS camera (Prime95B; Teledyne Photometrics, Tucson, AZ, USA). The microscope was controlled via CELLSENS DIMENSION software (Olympus). For wide-field laser excitation of SecYEG-Atto 647N, 638 nm laser was used (Cobolt MLD-06 638 nm; Cobolt AB, Solna, Sweden). This was combined with a multiband pass dichroic splitter for excitation (Di03-R405/488/561/635-t1-25 × 36, Semrock, IDEX Co., West Henrietta, NY, USA) and the emitted light was filtered by a 635-nm-long pass filter (BLP01-635R-25, Semrock, IDEX Co.). For illumination during CPB experiments with DOPE-NBD a solid-state white light source (Lumencor SOLA SE 2; Lumencor, Beaverton, OR, USA) was used together with a 482/18 nm single-band bandpass filter (FF02-482/18–25; Semrock, IDEX Co.). The reflected light was filtered by a 525/39 nm single-band bandpass filter (FF01-525/39–25; Semrock, IDEX Co.).

Measurement of SLB mobility with continuous photobleaching

Lipid mobility within the SLB was probed via CPB following a previously published protocol [68]. With this technique, the lateral diffusion constant of DOPE-NBD in the bilayer is measured. Photobleaching occurs during continuous observation of fluorescent labels. As long as lipids within the bilayer are mobile, bleached fluorophores coupled to lipids can be replaced by fresh ones due to diffusion. Quantitative evaluation of the bleaching rate of fluorophores and of the intensity profile at the rim of the illuminated area enables extraction of the diffusion constant. The illumination field stop was opened to about 100 μm, and the illuminated area was bleached after prolonged exposure. Depending on the lipid mobility a bright rim was visible at the edges. To determine the bleaching constant, B, the average intensity in a square area (0.55×0.55 μm^2) in the center of the illuminated area was fitted with Eqn (1):

$$I(t) = I_0 e^{-\mathrm{Bt}} + I_{\mathrm{Bg}}, \quad (1)$$

where I_0 is the initial intensity, I_{Bg} is the background intensity, and B is the bleaching constant, which are fitting parameters. By knowing B, the diffusion constant D could be extracted from the spatial intensity distribution. To do this, a mean intensity curve $I(r)$ was calculated from the intensity distribution averaged over a five-pixel wide line drawn perpendicular to the edge of the field stop. This was then fitted with Eqn (2).

$$I(r) = I_0 e^{-\mathrm{xA}} + I_{\mathrm{Bg}}, \quad (2)$$

where $A = \sqrt{B/D}$, I_0 and I_{Bg} as before. From each bleached area, along four radial lines the diffusion constants were calculated from A and B. The images were taken at a rate of 1 Hz at exposure time of 0.5 s. The analysis was automated using self-written routines in Matlab (R2018a; MathWorks Inc., Natick, MA, USA).

Total internal reflection fluorescence microscopy

TIRFm measurements were performed at room temperature on an Olympus IX-71 microscope equipped a 100× oil-objective UApoN, NA 1.49 (Olympus) and set to TIRF-illumination ($\Theta < \Theta_c$) equipped with a DV2 multichannel imaging system (Teledyne Photometrics) with 537/29 and 610/75 ET band pass filters and a zt561RDC mirror (Chroma Technology Corp., Bellows Falls, VT, USA). SecYEG-Atto 647N were excited by 638 nm continuous-wave laser (Coherent Inc., Santa Carla, CA, USA) at approximately 1 kW·cm^{-2}. Images were captured using a 512 × 512 pixel electron multiplying charge coupled device camera C9100-13 (Hamamatsu Photonics) with EM-gain set to 254 at 33 frames·second^{-1} (temporal resolution 30 ms) and METAVUE imaging software (Molecular Devices LLC, San Jose, CA, USA).

Data acquired in TIRFm measurements were analyzed with IMAGEJ v1.48 using built-in and purpose-built plugins. Data were visualized using ORIGINPRO v9.1 (OriginLab Corp., Northampton, MA, USA) and MATLAB R2016b (MathWorks Inc.). To localize and track fluorescently labeled translocons, images were processed using a discoidal averaging filter with an inner and outer radius of one and four pixels, respectively [69]. Next, local fluorescence maxima which intensities exceeded either fixed or dynamic threshold (see below), and which were separated by at least four pixels, were selected. A two-dimensional Gaussian model was fitted to each point-spread functions (PSF) on the original unprocessed image by minimizing the RSS value by means of the Levenberg-Marquardt algorithm [70,71]. The resulting Gaussian model gave the amplitude, subpixel coordinates, symmetrical spread localization accuracy, and goodness of fit of the peak positions for each frame below the diffraction limit with an accuracy of 10–20 nm.

Oligomeric state of SecYEG

To investigate the oligomeric state of SecYEG particles in SLB, foci were detected using a fixed gray value threshold to minimize the dynamic threshold filtering artefacts caused by local background intensity changes. The fixed threshold value was based on the intensities of particles in the last recorded frames, where bleaching positively affected the background fluorescence, and where the remaining fluorescence represented an estimation of a single-molecule intensity. Signals passing the threshold were fitted to a two-

dimensional Gaussian model by minimizing the RSS value by means of the Levenberg-Marquardt algorithm. The obtained amplitude and PSF were used to calculate the Gaussian integral for each foci in the last 100 frames of multiple movies (Eqn 3). The obtained values were plotted in a histogram and fitted with a 2D Gaussian, of which the peak maximum represented the average integrated Gaussian intensity of a single molecule.

$$\int_{-\infty}^{\infty}\int_{-\infty}^{\infty} f(x,y)dxdy = 2\pi A\sigma_x\sigma_y. \quad (3)$$

Subpixel coordinates were obtained from particles, upon which a selection with a radius of two pixels from the centroid was made. From this selection, the raw integrated density was calculated and divided by the integrated Gaussian intensity of a single molecule, resulting in the number of molecules per focus.

Membrane diffusion behavior of SecYEG

To study the diffusional behavior of SecYEG, particles were detected using a dynamic threshold. The dynamic threshold was defined as $-x + 6*\sigma$, where $-x$ and σ are the average and standard deviation of the background gray value, respectively. The peak location data were filtered to exclude poorly fitted peaks (adjusted RSS < 0.2), after which the remaining coordinates were used to create particle trajectories by linking particles located nearest to each other in consecutive frames. A maximum step size constraint of three pixels was used to prevent linkage of particles too far apart to be the same. The step sizes constituting these trajectories were filtered on a minimal displacement of 0.06 $\mu m^2 \cdot s^{-1}$ to filter out artefacts, for example false linkages and immobile molecules, and the trajectories were filtered on the fitting accuracy of at least 20 nm trajectory lengths, and the particle displacement. The resulting data set consisting out of approximately 5000–10 000 step sizes per movie, contained only the coordinates of moving particles, which were further used for calculation of the CPD of step sizes. In short, a probability density function was created from the step size data and normalized resulting in the CPD. To extract the SecYEG diffusion characteristics, the CPD was fitted to the multicomponent CPD function (CPF, Eqn 4):

$$P(r^2,\tau) = 1 - \alpha e^{\left(\frac{-r^2}{\langle r_\alpha^2\rangle + 4\sigma^2}\right)} - \beta e^{\left(\frac{-r^2}{\langle r_\beta^2\rangle + 4\sigma^2}\right)} - \gamma e^{\left(\frac{-r^2}{\langle r_\gamma^2\rangle + 4\sigma^2}\right)}, \quad (4)$$

where α, β, and γ are the fraction of each population with the constraints that the sum of fractions cannot exceed 1. $\langle r^2_{\alpha,\beta,\gamma}\rangle$ give the MSD for each population at each time point (τ). The localization accuracy, σ, was determined from the mean error in the x and y parameters from the Gaussian fit. The CPF goodness-of-fit was determined by calculating the RSS value. The MSD of the best fitting model (RSS close to 0) was used to calculate the diffusion coefficient from the slope by plotting the obtained MSD value as a function of time.

Acknowledgement

This work was supported by the Netherlands Organization of Scientific Research in Earth and Life Sciences (NWO-ALW) and by the Foundation for Fundamental Research on Matter (FOM/NWO-I) to AJMD. AK acknowledges the support from the German Research Foundation (Deutsche Forschungsgemeinschaft, DFG; project ID Ke1879/3-1). CM acknowledges the support from VolkswagenFoundation (Freigeist fellowship, project ID 94195). AK and CM acknowledge the support within the DFG Collaborative Research Center 1208 'Identity and dynamics of biological membranes' (project ID 267205415). Open access funding enabled and organized by ProjektDEAL.

Conflicts of interest

The authors declare no conflict of interest.

Author contributions

All authors conceived the idea for the project and designed the experiments. SK and MK performed experiments including protein purification, lipid preparation, A-BS, SK, MK, and DK performed glass functionalization, microscopy experiments and data analysis. AK isolated RNCs and performed nanodisc-based experiments. CM, AJMD, and AK supervised the work. All authors contributed to writing and editing of the manuscript and approved the final version.

Peer Review

The peer review history for this article is available at https://publons.com/publon/10.1111/febs.15596.

References

1 Park E & Rapoport TA (2012) Mechanisms of Sec61/SecY-mediated protein translocation across membranes. *Annu Rev Biophys* **41**, 21–40.
2 Plessis DJF, Nouwen N & Driessen AJM (2011) The Sec translocase. *Biochim Biophys Acta* **1808**, 851–865.
3 Hegde RS & Bernstein HD (2006) The surprising complexity of signal sequences. *Trends Biochem Sci* **31**, 563–571.

4 Akopian D, Shen K, Zhang X & Shan S (2013) Signal recognition particle: an essential protein-targeting machine. *Annu Rev Biochem* **82**, 693–721.
5 Niesen M, Muller-Lucks A, Hedman R, von Heijne G & Miller TFI (2018) Forces on nascent polypeptides during membrane insertion and translocation via the Sec translocon. *Biophys J* **115**, 1885–1894.
6 Hoffmann A, Bukau B & Kramer G (2010) Structure and function of the molecular chaperone Trigger factor. *Biochim Biophys Acta Mol Cell Res* **1803**, 650–661.
7 Huber D, Jamshad M, Hanmer R, Schibich D, Döring K, Marcomini I, Kramer G & Bukau B (2017) SecA cotranslationally interacts with nascent substrate proteins *in vivo*. *J Bacteriol* **199**, e00622-16.
8 Sala A, Bordes P & Genevaux P (2014) Multitasking SecB chaperones in bacteria. *Front Microbiol* **5**, 666.
9 Tanaka Y, Sugano Y, Takemoto M, Mori T, Furukawa A, Kusakizako T, Kumazaki K, Kashima A, Ishitani R, Sugita Y *et al*, (2015) Crystal structures of SecYEG in lipidic cubic phase elucidate a precise resting and a peptide-bound state. *Cell Rep* **13**, 1561–1568.
10 Fröderberg L, Houben E, Samuelson JC, Chen M, Park S-K, Phillips GJ, Dalbey R, Luirink J & de Gier JWL (2003) Versatility of inner membrane protein biogenesis in *Escherichia coli*. *Mol Microbiol* **47**, 1015–1027.
11 Wu ZC, De Keyzer J, Kedrov A & Driessen AJM (2012) Competitive binding of the SecA ATPase and ribosomes to the SecYEG translocon. *J Biol Chem* **287**, 7885–7895.
12 Shen HH, Lithgow T & Martin LL (2013) Reconstitution of membrane proteins into model membranes: seeking better ways to retain protein activities. *Int J Mol Sci* **14**, 1589–1607.
13 Cross TA, Sharma M, Yi M & Zhou HX (2011) Influence of solubilizing environments on membrane protein structures. *Trends Biochem Sci* **36**, 117–125.
14 Van Der Does C, Swaving J, Van Klompenburg W & Driessen AJM (2000) Non-bilayer lipids stimulate the activity of the reconstituted bacterial protein translocase. *J Biol Chem* **275**, 2472–2478.
15 Van Der Laan M, Houben ENG, Nouwen N, Luirink J & Driessen AJM (2001) Reconstitution of Sec-dependent membrane protein insertion: nascent FtsQ interacts with YidC in a Sec YEG-dependent manner. *EMBO Rep* **2**, 519–523.
16 Taufik I, Kedrov A, Exterkate M & Driessen AJM (2013) Monitoring the activity of single translocons. *J Mol Biol* **425**, 4145–4153.
17 Koch S, De Wit JG, Vos I, Birkner JP, Gordiichuk P, Herrmann A, Van Oijen AM & Driessen AJM (2016) Lipids activate SecA for high affinity binding to the SecYEG complex. *J Biol Chem* **291**, 22534–22543.
18 Kater L, Frieg B, Berninghausen O, Gohlke H, Beckmann R & Kedrov A (2019) Partially inserted nascent chain unzips the lateral gate of the Sec translocon. *EMBO Rep* **20**, e48191.
19 Koch S, Driessen AJM & Kedrov A (2018) Biophysical analysis of Sec-mediated protein translocation in nanodiscs. In Advances in Biomembranes and Lipid Self-Assembly (Iglič A, Rappolt M & García-Sáez AJ, eds.), Vol. **28**, pp. 41–85. Elsevier Science, Amsterdam.
20 Haruyama T, Sugano Y, Kodera N, Uchihashi T, Ando T, Tanaka Y, Konno H & Tsukazaki T (2019) Single-unit imaging of membrane protein-embedded nanodiscs from two oriented sides by high-speed atomic force microscopy. *Structure* **27**, 152–160.e3.
21 Brian AA & McConnell HM (1984) Allogeneic stimulation of cytotoxic T cells by supported planar membranes. *Proc Natl Acad Sci USA* **81**, 6159–6163.
22 Cho NJ, Frank CW, Kasemo B & Höök F (2010) Quartz crystal microbalance with dissipation monitoring of supported lipid bilayers on various substrates. *Nat Protoc* **5**, 1096–1106.
23 Matysik A & Kraut RS (2014) Preparation of mica supported lipid bilayers for high resolution optical microscopy imaging. *J Vis Exp* **88**, e52054.
24 Nguyen PA, Field CM, Groen AC, Mitchison TJ & Loose M (2015) Using supported bilayers to study the spatiotemporal organization of membrane-bound proteins. *Methods Cell Biol* **128**, 223–241.
25 Gari RRS, Chattrakun K, Marsh BP, Mao C, Chada N, Randall LL & King GM (2019) Direct visualization of the *E. coli* Sec translocase engaging precursor proteins in lipid bilayers. *Sci Adv* **5**, eaav9404.
26 Karner A, Nimmervoll B, Plochberger B, Klotzsch E, Horner A, Knyazev DG, Kuttner R, Winkler K, Winter L, Siligan C *et al*, (2017) Tuning membrane protein mobility by confinement into nanodomains. *Nat Nanotechnol* **12**, 260–266.
27 García-Sáez AJ & Schwille P (2010) Surface analysis of membrane dynamics. *Biochim. Biophys Acta Biomembr* **1798**, 766–776.
28 Bianchi F, Syga L, Moiset G, Spakman D, Schavemaker PE, Punter CM, Seinen AB, Van Oijen AM, Robinson A & Poolman B (2018) Steric exclusion and protein conformation determine the localization of plasma membrane transporters. *Nat. Commun* **9**, 501.
29 Kiessling V & Tamm LK (2003) Measuring distances in supported bilayers by fluorescence interference-contrast microscopy: polymer supports and SNARE proteins. *Biophys J* **84**, 408–418.
30 Nováková E, Giewekemeyer K & Salditt T (2006) Structure of two-component lipid membranes on solid support: an X-ray reflectivity study. *Phys Rev E Stat Nonlin Soft Matter Phys* **74**, 051911.
31 Zhu M, Lerum MZ & Chen W (2012) How to prepare reproducible, homogeneous, and hydrolytically stable aminosilane-derived layers on silica. *Langmuir* **28**, 416–423.

32 Macháň R & Hof M (2010) Lipid diffusion in planar membranes investigated by fluorescence correlation spectroscopy. *Biochim Biophys Acta Biomembr* **1798**, 1377–1391.

33 Kedrov A, Kusters I, Krasnikov VV & Driessen AJM (2011) A single copy of SecYEG is sufficient for preprotein translocation. *EMBO J* **30**, 4387–4397.

34 Dalal K, Chan CS, Sligar SG & Duong F (2012) Two copies of the SecY channel and acidic lipids are necessary to activate the SecA translocation ATPase. *Proc Natl Acad Sci USA* **109**, 4104–4109.

35 Gold VAM, Robson A, Bao H, Romantsov T, Duong F & Collinson I (2010) The action of cardiolipin on the bacterial translocon. *Proc Natl Acad Sci USA* **107**, 10044–10049.

36 Becker T, Bhushan S, Jarasch A, Armache JP, Funes S, Jossinet F, Gumbart JC, Mielke T, Berninghausen O, Schulten K *et al*, (2009) Structure of monomeric yeast and mammalian Sec61 complexes interacting with the translating ribosome. *Science* **326**, 1369–1373.

37 Park E & Rapoport TA (2012) Bacterial protein translocation requires only one copy of the SecY complex *in vivo*. *J Cell Biol* **198**, 881–893.

38 Gong F & Yanofsky C (2002) Instruction of translating ribosome by nascent peptide. *Science* **297**, 1864–1867.

39 Saffman PG & Delbrück M (1975) Brownian motion in biological membranes. *Proc Natl Acad Sci USA* **72**, 3111–3113.

40 Kuznetsova IM, Turoverov KK & Uversky VN (2014) What macromolecular crowding can do to a protein. *Int J Mol Sci* **15**, 23090–23140.

41 Ma C, Wu X, Sun D, Park E, Catipovic MA, Rapoport TA, Gao N & Li L (2019) Structure of the substrate-engaged SecA-SecY protein translocation machine. *Nat Commun* **10**, 2872.

42 Milon S, Hovius R, Vogel H & Wohland T (2003) Factors influencing fluorescence correlation spectroscopy measurements on membranes: Simulations and experiments. *Chem Phys* **288**, 171–186.

43 Matysik A & Kraut RS (2014) TrackArt: The user friendly interface for single molecule tracking data analysis and simulation applied to complex diffusion in mica supported lipid bilayers. *BMC Res Notes* **7**, 274.

44 Miller CE, Majewski J, Gog T & Kuhl TL (2005) Characterization of biological thin films at the solid-liquid interface by X-ray reflectivity. *Phys Rev Lett* **94**, 238104.

45 Sackmann E (1996) Supported membranes: scientific and practical applications. *Science* **271**, 43–48.

46 Hamai C, Yang T, Kataoka S, Cremer PS & Musser SM (2006) Effect of average phospholipid curvature on supported bilayer formation on glass by vesicle fusion. *Biophys J* **90**, 1241–1248.

47 Michalet X (2010) Mean square displacement analysis of single-particle trajectories with localization error: Brownian motion in an isotropic medium. *Phys Rev E Stat Nonlin Soft Matter Phys* **82**, 041914.

48 Ritchie K, Iino R, Fujiwara T, Murase K, Kusumi A, Ritchie K, Iino R, Fujiwara T & Murase K (2003) The fence and picket structure of the plasma membrane of live cells as revealed by single molecule techniques. *Mol Membr Biol* **20**, 13–18.

49 Sarangi NK, Ayappa KG & Basu JK (2017) Complex dynamics at the nanoscale in simple biomembranes. *Sci Rep* **7**, 11173.

50 Ott M, Shai Y & Haran G (2013) Single-particle tracking reveals switching of the HIV fusion peptide between two diffusive modes in membranes. *J Phys Chem B* **117**, 13308–13321.

51 Quemeneur F, Sigurdsson JK, Renner M, Atzberger PJ, Bassereau P & Lacoste D (2014) Shape matters in protein mobility within membranes. *Proc Natl Acad Sci USA* **111**, 5083–5087.

52 Kreutzberger AJB, Ji M, Aaron J, Mihaljević L & Urban S (2019) Rhomboid distorts lipids to break the viscosity-imposed speed limit of membrane diffusion. *Science* **363**, eaao0076.

53 Prabudiansyah I, Kusters I, Caforio A & Driessen AJM (2015) Characterization of the annular lipid shell of the Sec translocon. *Biochim Biophys Acta Biomembr* **1848**, 2050–2056.

54 Koch S, Exterkate M, López CA, Patro M, Marrink SJ & Driessen AJM (2019) Two distinct anionic phospholipid-dependent events involved in SecA-mediated protein translocation. *Biochim Biophys Acta Biomembr* **1861**, 183035.

55 Bischoff L, Wickles S, Berninghausen O, Van Der Sluis EO & Beckmann R (2014) Visualization of a polytopic membrane protein during SecY-mediated membrane insertion. *Nat Commun* **5**, 4103.

56 Nagamori S, Nishiyama K-I & Tokuda H (2002) Membrane topology inversion of SecG detected by labeling with a membrane-impermeable sulfhydryl reagent that causes a close association of SecG with SecA. *J Biochem* **132**, 629–634.

57 Frauenfeld J, Gumbart J, van der Sluis EO, Funes S, Gartmann M, Beatrix B, Mielke T, Berninghausen O, Becker T, Schulten K *et al*, (2011) Cryo-EM structure of the ribosome–SecYE complex in the membrane environment. *Nat Struct Mol Biol* **18**, 614–621.

58 Zimmer J, Nam Y & Rapoport TA (2008) Structure of a complex of the ATPase SecA and the protein-translocation channel. *Nature* **455**, 936–943.

59 Lill R, Dowhan W & Wickner W (1990) The ATPase activity of SecA is regulated by acidic phospholipids, SecY, and the leader and mature domains of precursor proteins. *Cell* **60**, 271–280.

60 Breukink E, Demel RA, de Korte-Kool G & de Kruijff B (1992) SecA insertion into phospholipids is stimulated by negatively charged lipids and inhibited by ATP: a monolayer study. *Biochemistry* **31**, 1119–1124.
61 Corey RA, Pyle E, Allen WJ, Watkins DW, Casiraghi M, Miroux B, Arechaga I, Politis A & Collinson I (2018) Specific cardiolipin–SecY interactions are required for proton-motive force stimulation of protein secretion. *Proc Natl Acad Sci USA* **115**, 7967–7972.
62 Prabudiansyah I, Kusters I & Driessen AJM (2015) *In vitro* interaction of the housekeeping SecA1 with the accessory SecA2 protein of Mycobacterium tuberculosis. *PLoS One* **10**, 0128788.
63 De Keyzer J, Van der Does C & Driessen AJM (2002) Kinetic analysis of the translocation of fluorescent precursor proteins into *Escherichia coli* membrane vesicles. *J Biol Chem* **277**, 46059–46065.
64 Kedrov A, Wickles S, Crevenna AH, van der Sluis EO, Buschauer R, Berninghausen O, Lamb DC & Beckmann R (2016) Structural dynamics of the YidC: ribosome complex during membrane protein biogenesis. *Cell Rep* **17**, 2943–2954.
65 Seidelt B, Innis CA, Wilson DN, Gartmann M, Armache JP, Villa E, Trabuco LG, Becker T, Mielke T, Schulten K *et al*, (2009) Structural insight into nascent polypeptide chain-mediated translational stalling. *Science* **326**, 1412–1415.
66 Allerbo O, Lundström A & Dimitrievski K (2011) Simulations of lipid vesicle rupture induced by an adjacent supported lipid bilayer patch. *Colloids Surfaces B Biointerfaces* **82**, 632–636.
67 Cremer PS & Boxer SG (1999) Formation and spreading of lipid bilayers on planar glass supports. *J Phys Chem B* **103**, 2554–2559.
68 Fenz SF, Merkel R & Sengupta K (2009) Diffusion and Intermembrane distance: case study of avidin and e-cadherin mediated adhesion. *Langmuir* **25**, 1074–1085.
69 Hedde PN, Fuchs J, Oswald F, Wiedenmann J & Nienhaus GU (2009) Online image analysis software for photoactivation localization microscopy. *Nat Methods* **6**, 689–690.
70 Levenberg K (1944) A method for the solution of certain non – linear problems in least squares. *Q Appl Math* **2**, 164–168.
71 Marquardt DW (1963) An algorithm for least-squares estimation of nonlinear parameters. *J Soc Ind Appl Math* **11**, 431–441.
72 Pettersen EF, Goddard TD, Huang CC, Couch GS, Greenblatt DM, Meng EC & Ferrin TE (2004) UCSF Chimera - a visualization system for exploratory research and analysis. *J Comput Chem* **25**, 1605–1612.